Cosmic-Ray Air Showers at Sea Level*

G. W. CLARK, J. EARL, W. L. KRAUSHAAR, J. LINSLEY, B. B. ROSSI, F. SCHERB, AND D. W. SCOTT
Laboratory for Nuclear Science, Massachusetts Institute of Technology, Cambridge, Massachusetts

(Received December 13, 1960)

An investigation at sea level of cosmic-ray showers with sizes from 5×10^5 to over 10^9 particles is described. The core locations, arrival directions, and particle density distributions of several thousand showers whose cores landed within an area of 10^5 m^2 were determined by the techniques of fast-timing and density sampling. The most important results are as follows: (1) The existence of primary particles with energies greater than 10^{18} ev is established by the observation of one shower with more than 10^9 particles. (2) The function $f(r)=0.45(N/R_0^2)r^{-0.7}(1+r)^{-3.2}$, where $r=R/R_0$ and $R_0=79$ m, describes the lateral distribution of particles at distances in the range $50\text{ m}<R<400$ m and for showers with sizes in the range $5\times10^5<N<10^8$. (3) At distances greater than 50 m from the core the density fluctuations in individual showers have a Poisson distribution. (4) The size and zenith angle distribution can be represented by the formula $s(N,x)=s_0(10^6/N)^{\Gamma+1}\exp[-(x-x_0)/\Lambda]$, where $x=x_0\sec\theta$, $x_0=1040$ g cm^{-2}, $s_0=(6.6\pm1.0)\times10^{-8}$ cm^{-2} sec^{-1} sterad^{-1}, $\Gamma=1.9\pm0.1$, $\Lambda=(113\pm9)$ g cm^{-2}, $x_0<x<1.3x_0$, and $7\times10^5<N<7\times10^8$. (5) No evidence is found of anisotropy in the arrival directions or of a break in the energy spectrum of the primaries up to the largest energies observed. (6) Assuming a specific model for shower development and taking into account fluctuations in the depth of the first interaction, the integral energy spectrum of the primaries is $J(E)=J_0(10^{15}/E)^\gamma$, where $J_0=(8.1\pm3.1)\times10^{-11}$ cm^{-2} sec^{-1} sterad^{-1}, $\gamma=2.17\pm0.1$, and 3×10^{15} ev $<E<10^{18}$ ev.

I. INTRODUCTION

THIS paper is a part of the final report[1] on an experimental investigation of air showers with sizes in the range from 5×10^5 to 10^9 particles at sea level. The work was carried out between 1954 and 1957 at the Agassiz Station of the Harvard College Observatory, and preliminary reports on the results have been given previously.[2–4]

The primary purpose of the experiment was to study the energy spectrum and arrival directions of ultra-high-energy primary cosmic rays for the sake of the information which these data give about the origin of cosmic rays. The secondary purpose was to obtain new and more accurate data on the structure of air showers themselves in order to provide criteria for judging the validity of shower theories based on models of ultra-high-energy interactions.

We strove to obtain as complete information as we could about each shower detected. We were able to determine rather accurately the size, core location, arrival direction and lateral particle distribution of each of many individual showers whose cores landed within a large array of detectors. This can be called a "high-resolution" approach, in contrast to others that yield only average values for showers with a broad range of characteristics. Investigation of the shower size spectrum by measurement of the density spectrum, a typical "low-resolution" technique, has the disadvantage that a sudden cutoff in the size spectrum would cause only gradual increase in the slope of the density spectrum over a range of a factor of 10 or more in densities.

Our experimental method was a combination of the techniques of fast-timing[5] and density sampling[6] which had been developed separately in previous air shower experiments in this laboratory. The first of these is based on the fact that the particles in a shower are concentrated in a thin disk normal to the axis, traveling along the axis with nearly the speed of light. Thus one can determine the direction of the axis from the relative arrival times of the shower particles at several widely separated detectors. The second is based on the fact that the particle density in a shower is circularly symmetric and decreases monotonically with distance from the axis. As we shall show, this permits one to determine the core location, lateral distribution, and shower size by analyzing the pattern of particle densities registered by the same detectors used for timing.

II. METHOD

The method underwent considerable evolution during the experiment. Only the final version will be described, since most of the final results were obtained with it.

A. Equipment

Large-area plastic scintillation detectors served the dual purpose of measuring particle densities and arrival times. The inset in Fig. 1 shows the construction of a detector. A plastic scintillator disk 42 in. in diameter and 3 in. thick[7] and a 5-in. Dumont type 6364 photomultiplier were enclosed in a cylindrical galvanized steel can painted white inside. Scintillation light could reach the photocathode only by reflection from the walls of the can. The light gathering efficiency of this arrangement showed a radial variation of a factor less than two between the center and edge of the scintillator. Figure 1 shows the response of a typical detector both to the sea

* This work was supported in part by the U. S. Atomic Energy Commission, the Office of Naval Research, and in part, also, by a grant from the National Science Foundation.

[1] The results of a study of the μ mesons associated with air showers will be published separately.

[2] G. Clark, J. Earl, W. Kraushaar, J. Linsley, B. Rossi, and F. Scherb, Nature **180**, 353 (1957).

[3] G. Clark, J. Earl, W. Kraushaar, J. Linsley, B. Rossi, and F. Scherb, Nuovo cimento Suppl. **8**, Ser. **10**, 623 (1958).

[4] B. Rossi, Proc. Cosmic Ray Conf. IUPAP, Moscow, 1959.

[5] P. Bassi, G. Clark, and B. Rossi, Phys. Rev. **92**, 441 (1953).

[6] R. W. Williams, Phys. Rev. **74**, 1689 (1948).

[7] G. W. Clark, F. Scherb, and W. Smith, Rev. Sci. Instr. **28**, 433 (1957).

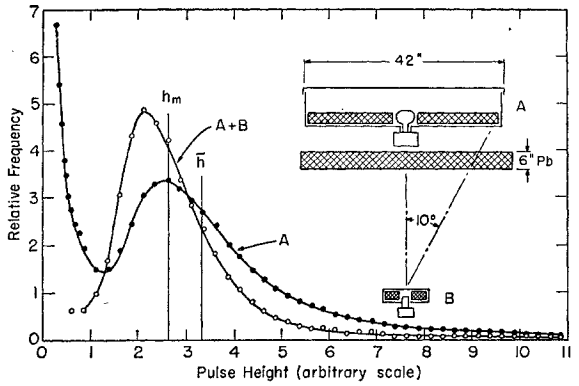

FIG. 1. Differential distributions in size for pulses from a 42-in. detector, with (curve "$A+B$") and without (curve "A") coincident pulses from another small detector under 6 in. of lead. The inset is a schematic diagram of the 42-in. detector and the coincidence arrangement whereby pulses due to single penetrating particles were selected to obtain curve "$A+B$." The vertical line labeled $\bar{h}$ marks the standard calibration pulse height defined so that the rate for pulses of height greater than $\bar{h}$ produced by uncollimated particles is 70 sec^{-1}. The vertical line labeled h_m marks the median height of pulses due to single penetrating nearly vertical particles.

level flux of cosmic rays and to collimated vertical penetrating particles.

In arranging the detectors to form an array there are conflicting requirements. For large showers low intensity is the problem; detectors must enclose a large sensitive area but may be placed rather far apart. For small showers counters must be spaced more closely, but the sensitive area need not be as great. During most of our experiment there were 11 detectors arranged in two concentric rings (M and D) with one

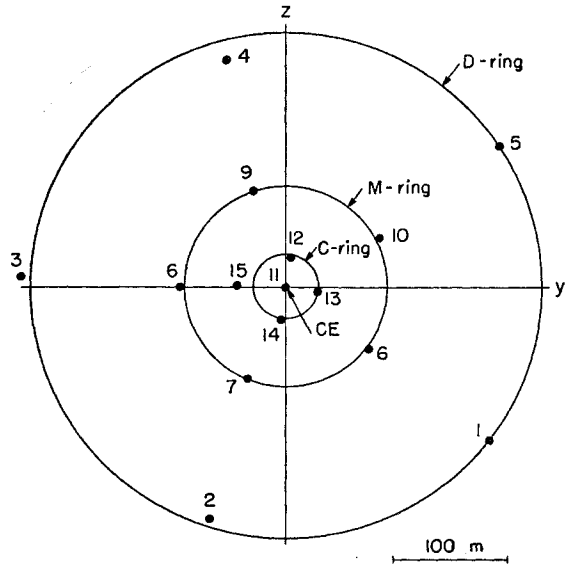

FIG. 2. Schematic diagram of the detector array. The four detectors in the C ring were used only during a small part of the running time in order to extend the results to showers as small as 5×10^5 particles.

at the center, as shown in Fig. 2. With this design relatively few detectors served to cover a wide range of shower sizes and a very wide range of intensities. For a short period four additional detectors in a small ring (C) were used to extend the survey to showers smaller than we could study with the normal arrangement.

Figure 3 is a block diagram of the electronic system used for selecting showers and recording data. The equalizer delay lines compensated for differences between the lengths of the transmission lines that connected the detectors to the central station. They were trimmed so that simultaneous pulses from the detectors would arrive simultaneously at the central station. The transmission lines were doubly shielded coaxial cable (RG71A/U). They also served to distribute high-voltage power to the photomultipliers.

One of the problems in determining shower size by density sampling is that the electronic equipment must have a very wide dynamic range in order to record particle densities both close to and far from shower cores. In the system shown this is achieved by providing four ranges for amplitude, which represents density. The signal from each detector goes to a separate channel consisting of amplifiers, delay lines, and attenuators. There are four different electrical paths through each channel, and each path has a different over-all amplification and delay. A single input pulse emerges at the output as four successively more amplified and more delayed pulses. A very large input pulse, which without attenuation would saturate the amplifiers, appears at the output in a prompt but greatly attenuated version before the later distorted versions appear. On the other hand, a very small input pulse is seen in its most amplified and most delayed version. In our system the variously delayed paths differed from one another in over-all gain by successive factors of five, and the useful dynamic range for each path was about 1:20. Thus the over-all dynamic range was about 1:2500.

The output of each channel, with its four versions of the scintillation pulse, was displayed on a separate cathode-ray tube. The cathode-ray tubes were driven by common sweep and intensifier signals. Fiducial marks separated by 5 μsec were placed near the start and finish of each sweep by blanking small portions of the trace. The first mark was the reference for measurements of relative arrival times; the second permitted comparisons of sweep speed between channels. A tracing of the projected photographic record of one event is shown in Fig. 4. The sweep speed of a dummy cathode-ray tube labeled "monitor" was measured for each event so that small time variations in sweep speed could be taken into account.

The triggering requirement was that sufficiently large signals be received almost simultaneously from at least three detectors. Most of the time the pulse size requirement corresponded to 10 particles m^{-2}. An

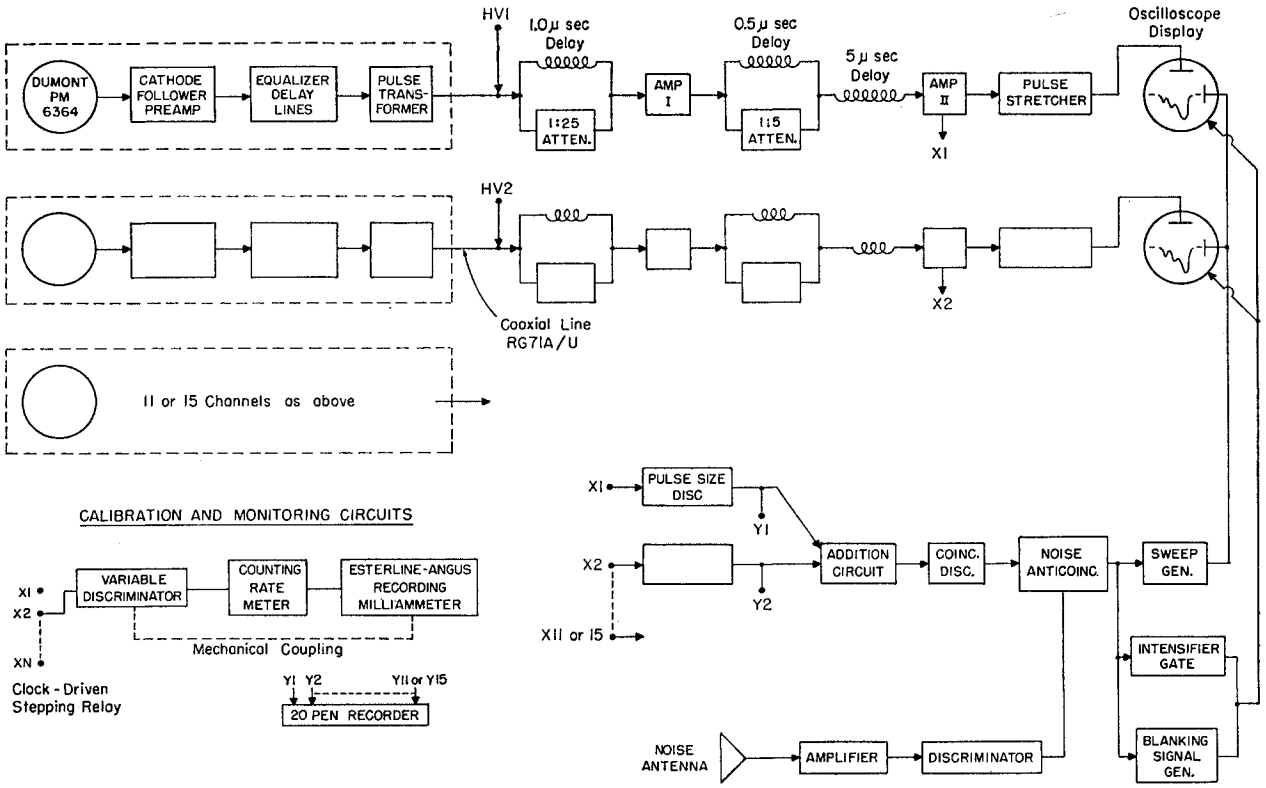

FIG. 3. Block diagram of the pulse recording system. Components within the dashed line were located at the detector sites.

anticoincidence circuit was used to reduce the number of false triggers produced by electrical storms. Its antenna was a coaxial cable strung out in the woods for several hundred meters.

A continuous cycle of calibrations was carried out automatically by a device consisting of a variable discriminator, a counting-rate meter, and a moving-chart pen recorder. The discriminator bias potentiometer was driven mechanically by the chart motor. Each detector channel was connected in turn to the discriminator by a stepping relay while its bias curve was recorded on the chart. In this way we obtained an integral cosmic-ray pulse height distribution for each detector three times daily. These pulse-height distributions were the basis for our shower density calibration and also were a means for detecting incipient faults. In addition we monitored the mounting rate of each pulse size discriminator using a multiple-pen recorder.

B. Calibration

To a good approximation the expected size of the pulse from a scintillation detector struck by a shower is proportional to the local density of shower particles and independent of the arrival direction of the shower. The proportionality comes from the fact that most shower particles are minimum ionizing so that the total output of scintillation light is proportional to the total track length. The scintillators were thin and composed of light elements equivalent to air so that there would be no significant transition effect. The density of particles within the plastic was therefore essentially the same as the density of incident particles. Pulse heights give a direct measure of shower density

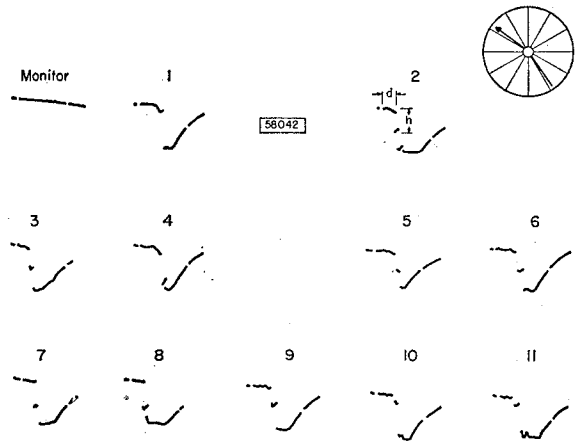

FIG. 4. Tracing of the photographic record for event number 58042, which was the largest shower recorded during the experiment. Above each oscilloscope trace is the number of the corresponding detector.

regardless of shower inclination because the decrease in projected target area for inclined showers is exactly compensated by the increased track length for each incident particle.

The calibration involved two steps: the first, to measure routinely the relative response of the detectors and their recording system to a standard scintillation event; the second, to relate the standard event to density of shower particles. The routine procedure made use of the automatically recorded bias curves mentioned above. The standard pulse height, called $\bar{h}$, corresponded to the bias level at which the counting rate for uncollimated cosmic rays was 70 sec^{-1}. Its position in the typical differential pulse-height distributions of collimated and uncollimated particles is shown in Fig. 1. The reference pulse size thus defined is not an ideal standard since the intensity of sea level cosmic rays is not perfectly constant. However, the real changes in sensitivity of our detectors were much larger than the apparent changes (amounting to 1 or 2%) that would be produced by normal variations in cosmic-ray intensity. The real changes in sensitivity were chiefly temperature effects. Direct measurements of the temperature coefficient of $\bar{h}$ for various detectors gave values in the range -0.3 to -1% per °C. Typical day-night temperature excursions at the Agassiz site were 10°C. The effect of the resulting 3 to 10% diurnal variation in detector sensitivity on our study of arrival directions was insignificant compared to statistical errors.

Two approaches were used in relating the working pulse-height standard to particle density. The first was to compare $\bar{h}$ with the median size h_m of pulses produced by nearly vertical penetrating particles traversing the detector at positions distributed randomly over its area. As Fig. 1 shows, $\bar{h}$ is larger than h_m by the factor $\bar{h}/h_m=1.25\pm0.05$ where the error reflects the estimated error in that particular measurement of $\bar{h}$.

The second approach was to compare nominal particle densities measured with the plastic scintillation detectors to densities measured by standard Geiger tube techniques. By "nominal" densities we mean densities measured in units of our $\bar{h}$. To make this comparison we installed a hodoscoped tray of 96 unshielded Geiger tubes near a scintillation detector of the C ring and recorded Geiger tube discharges in coincidence with showers detected by our normal method. For each shower in this run we found the expected nominal density g at the position of the Geiger tray from the arrival direction, core location, and nominal size, calculated by the procedure we will later describe. In effect, g was an interpolated density obtained by fitting an assumed lateral distribution function to the nominal densities measured at the various points of the array. We selected 23 showers whose cores landed between 20 and 100 m from the test position and whose axes were within 20° of vertical. The number of Geiger counters expected to be discharged by the ith shower is $96[1-\exp(-kg_ia)]$, where a is the area of each Geiger tube (0.0300 m^2) and k is the ratio of the "Geiger tube density" to the nominal density g_i. The total number of Geiger tubes expected to be discharged is therefore $\sum_{i=1}^{23} 96[1-\exp(kg_ia)]$. Equating this to the observed number and solving for k we obtained the value $k=1.30\pm0.10$. Most of the error arises from uncertainty in the g_i values. A statistical analysis of the hodoscope record indicated there was no correlation between the discharge of adjacent tubes. The value of k is the same as the ratio $\bar{h}/h_m$ within the experimental errors.

Among our results only absolute shower intensities depend significantly on distinguishing between nominal shower size and Geiger tube size. It will be convenient for us to carry through most of our discussion in terms of nominal densities and sizes. The terms density and size should be understood to mean nominal density and size unless there is an explicit statement to the contrary. When we deal with the size spectrum we will make the distinction.

C. Reduction of Data

We projected the photographic record of each event onto a sheet of graph paper and measured the height and horizontal position of the most suitable version of each pulse. These data, together with the time of day, the day of the year, calibration data, and various instrumental and astronomical constants, were processed by automatic electronic computation. The basic idea was to find a set of shower parameters that described the circularly symmetric shower disk and that fitted the observed data according to the method of least squares.

The direction of the shower was found from the data on the relative arrival times. The computer determined algebraically the values of l, m, and t_0 that minimized the function

$$\chi^2=(q-3)^{-1}\sum(ct_i+ly_i+mz_i-ct_0)^2, \qquad (1)$$

where t_i is the relative arrival time at the ith detector, whose rectangular coordinates are y_i and z_i; l and m are the direction cosines of the shower axis; t_0 is the mean arrival time; q is the number of detectors from which

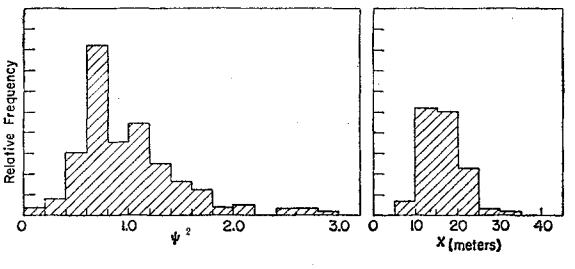

FIG. 5. Distributions in ψ^2 (density fit) and χ (timing fit) for 200 showers analyzed with the trial function NKA 1.4.

TABLE I. Specifications of artificial showers used to test the analysis procedure.

Test Sample	Number of showers	Size (particles)	Zenith angle	Azimuth	Core location
1	20	5×10^7	0°	···	Random within circle of radius 180 m.
2	20	5×10^7	30°	Random	Random within annular ring with radii 100 m and 180 m.
3	20	5×10^8	30°	Random	Random within annular ring with radii 180 m and 200 m.

timing information was obtained; and c is the speed of light. The zenith angle, right ascension, and declination were then computed from l and m.

The core location and size were determined from the density data, taking into account the inclination of the shower. A core position with rectangular coordinates Y, Z, and a size N were found that approximately minimized the function

$$\psi^2=(p-3)^{-1}\sum(\Delta_i'-g_i)^2W_i, \tag{2}$$

where Δ_i' is the calculated density for the ith detector, g_i is the observed density, W_i is the weighting factor, and p is the number of detectors from which density information was obtained. The calculated densities were related to the size and core position by the equation

$$\Delta_i'=(N/R_0^2)F(r_i), \tag{3}$$

where F is a trial lateral distribution function, R_0 is the Molière unit of length (79 m at sea level), and $r_i=R_i/R_0$. R_i is the perpendicular distance from the shower axis to the ith detector. The trial function has the usual normalization $\int_0^\infty F(r)2\pi r dr=1$ so that N represents the total number of particles. The weighting factor W_i is defined by the equation

$$W_i=[(\xi\Delta_i')^2+(\Delta_i'/A')]^{-1}, \tag{4}$$

where A' is the projected area of the detector and ξ is the fractional experimental error in an individual density measurement, estimated to be 0.15. The weighting factor was constructed to take proper account of both the Poisson fluctuations in the numbers of particles that traverse the detectors and the random instrumental errors.

Equation (2) defines a hypersurface which has a minimum for some set of values of Y, Z, and N. The calculation of this set of values was carried out by a series of successive approximations that began with rough initial estimates and terminated when certain numerical tests indicated that ψ^2 had been approximately minimized.

At various stages in our analysis we employed several different trial functions which we refer to as EXP, NKA 1.4, and NKGs.[8] These functions are defined as follows:

$$\mathrm{EXP}(r)=\exp(-r)/2\pi r, \tag{5a}$$

$$\mathrm{NKA\ 1.4}(r)=1.95r^{-1}(r+2)^{-3.33}, \tag{5b}$$

$$\mathrm{NKGs}(r)=C(s)r^{s-2}(r+1)^{s-4.5}. \tag{5c}$$

An approximate formula for the normalization factor $C(s)$ is $C(s)=0.443s^2(1.90-s)$. The function NKGs has been used by Greisen[9] to represent results of theoretical calculations by Nishimura and Kamata for purely electronic cascades.

D. Evaluation of the Data Reduction Procedure

The distributions of χ and ψ^2 for 200 showers analyzed with the trial function NKA 1.4 are shown in Fig. 5.

We tested the effect of fluctuations and errors in the data on computed direction and size by analyzing test samples of artificial shower data made up as indicated in Table I. Azimuths and core locations were chosen with the aid of a table of random numbers. Expected particle densities and arrival times were then calculated for each of the detector positions. To the expected densities we added random Poisson fluctuations, and then superimposed random Gaussian fluctuations with a standard deviation of 15% to take into account instrumental errors. To the arrival times we added Gaussian fluctuations with a standard deviation of 0.05 μsec, the value found for real showers by analysis of the distribution in χ. The artificial data were then analyzed in the usual way and the calculated shower parameters compared with those originally assumed.

Figure 6 is a target pattern for test samples 2 and 3

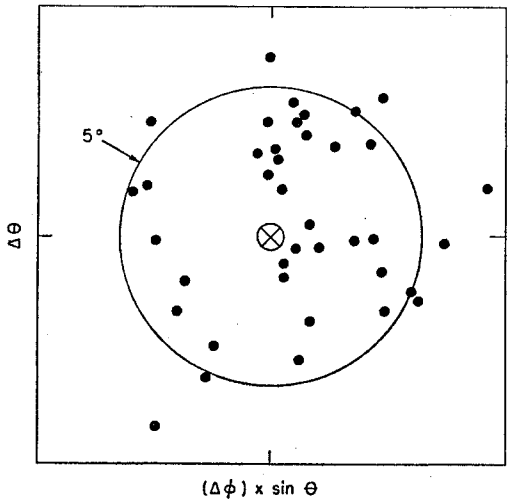

FIG. 6. Scatter of calculated arrival directions with respect to specified arrival directions for artificial showers with zenith angles equal to 30° and azimuth angles chosen at random (test samples 2 and 3). The components of each point represent the errors in the calculated values of θ and ϕ.

[8] EXP, NKA 1.4, NKGs stand for "exponential," "Nishimura-Kamata, approximate," and "Nishimura-Kamata, Greisen approximation," respectively.

[9] K. Greisen, *Progress in Cosmic Ray Physics*, edited by J. G. Wilson (North-Holland Publishing Company, Amsterdam, 1956), Vol. III, Chap. 1.

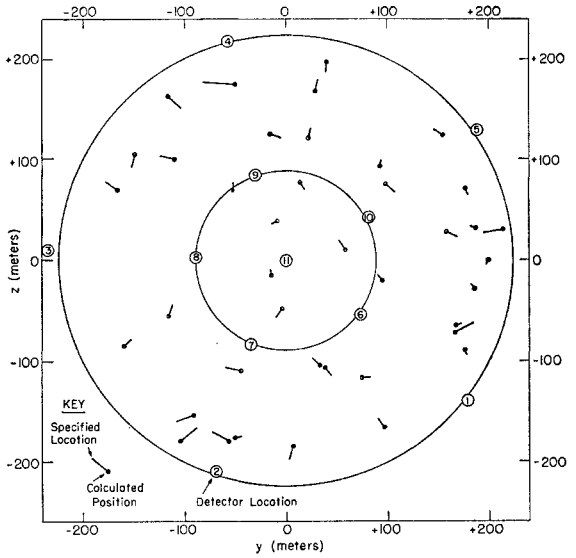

FIG. 7. Errors in calculated core positions for artificial showers. The dots represent the calculated core positions and the line segments the displacements from specified to calculated position. Open and solid dots are for sizes 5×10^7 and 5×10^8, respectively.

in which calculated arrival directions are represented by points displaced from the origin by distances proportional to the angular error. The average angular error is less than 5°. A similar result was obtained for the vertical artificial showers.

The errors in core location are shown in Fig. 7. For each shower we have drawn a line from the specified location to a dot representing the calculated location. The error displacements are random in direction. Their average magnitude is 6 m within the M ring and 11 m between the M and D rings. Additional tests on artificial showers with specified core locations outside the D ring of detectors revealed a tendency for the error in calculated position to be an inward displacement. To avoid systematic errors due to this effect we generally ignored showers whose calculated core positions were further than 190 m from the center. However, in view of the relatively large sensitive area lying on the fringes of the array it was to be expected that the cores of the largest and most rarely detected showers would fall in the fringe region where special attention had to be given in order to salvage the important information they furnish.

Figure 8 shows the distribution of errors in size. No significant systematic error is evident, and there is only a small deterioration in accuracy for core locations near the outer ring of detectors. The standard deviations of the calculated from the specified sizes are 9, 11, and 14% for test samples 1, 2, and 3, respectively.

In summary, the results on artificial showers indicate that the fluctuations in the timing and density data for real showers propagated through the analysis procedure can be expected to introduce the following random errors in the calculated shower parameters: (a) an average error in arrival direction less than 5°. (b) an average error in core location of about 10 m. (c) a standard deviation in size determination of about 10%. In addition to these errors one may anticipate systematic errors caused by any difference that may exist between the trial lateral distribution function and the true average lateral distribution function of the showers. Such errors will be discussed in relation to the experimental results on the lateral distribution.

III. EXPERIMENTAL RESULTS

When we began this experiment, the available theoretical and experimental information on the lateral density distribution of particles in extensive air showers was relatively crude. With our experimental method the problem of determining the core locations, the sizes, and the lateral density distributions are closely interrelated. Therefore, we had to proceed by successive approximations. We first carried out a preliminary analysis of the data using the trial function EXP as a crude approximation to the structure function. On the basis of the preliminary analysis we selected a better trial function, NKA 1.4, that we used in the final analysis from which all of the results on showers with sizes greater than 4×10^6 particles were obtained. Most of the results on smaller showers were obtained, however, using only the EXP trial function.

A. Average Lateral Distribution

The average density Δ of particles at a perpendicular distance R from the axis of a shower of size N will be expressed by the relation

$$\Delta=(N/R_0^2)f(r), \tag{6}$$

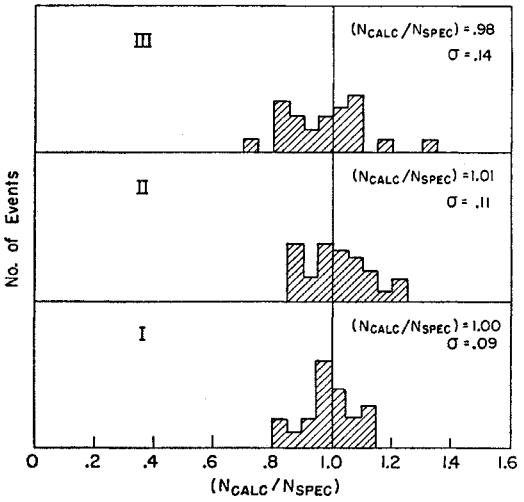

FIG. 8. Distributions of errors in shower size for the three test samples of artificial showers.

where $r=R/R_0$, R_0 is the Molière unit of length (79 m at sea level) and $f(r)$ is the so-called structure function.

In principle, the lateral distribution at a given elevation may depend on shower size and inclination. For our final determinations we selected samples of events according to the criteria listed in Table II. Sample 1, consisting of small showers with large zenith angles, represents the oldest showers we could study. The showers of sample 2 are again inclined but have been chosen somewhat larger so that better accuracy could be obtained for $r>1$. Sample 4 represents the largest showers available to us for this type of analysis. The inclinations are not very great. Sample 3 resembles sample 4 except that the showers are somewhat smaller. More showers were available in that size range.

The procedure for evaluating the average structure functions for a given sample made use of the following data printed out by the computer for each detector in each shower event: (1) the measured density g, (2) the calculated perpendicular distance r from the axis, and (3) the calculated density Δ' expected according to the calculated shower parameters and the assumed trial structure function F. Each event yielded 11 (samples 2, 3, and 4) or 15 (sample 1) measured and expected densities at distances generally ranging from a few meters to over 300 m from the shower axis. Thus we had available in each sample many pairs (g,Δ') of measured and calculated densities. We divided r into several equal logarithmic intervals, each one of which covered a range of a factor of 1.5. We put each pair of densities into one of several groups corresponding to the logarithmic interval into which the calculated distance r fell. We then found the ratio $(\bar{g}/\bar{\Delta}')_n$ of the average measured density $\bar{g}$ to the average expected density $\bar{\Delta}'$ for the nth interval. Presumably, if the trial function F were a good representation of the true structure function f, then the expected value of this ratio would be unity for all distance intervals. In fact, for both trial function EXP and NKA 1.4 we found small systematic deviations of this ratio from unity.

In Fig. 9 we have plotted these results for the various samples as points, each one of which has an abscissa equal to the arithmetic midpoint $\bar{r}_n$ of the interval of r, and an ordinate equal to the corresponding value of the quantity $(\bar{g}/\bar{\Delta}')_n \bar{r}_n F(\bar{r}_n)$. The resulting sets of points indicate the shapes of the average structure functions. The smooth curve drawn in each figure represents the normalized function NKG 1.3 multiplied by an adjusting factor which gives a good fit to the data points. The fact that the fitting factor is 1.00 for samples 2 and 3 indicates that the calculated sizes of showers in these samples are, on the average, correct. On the other hand, the fitting factors for samples 1 and 4 are not unity and are, in fact, the factors by which the calculated sizes of showers in these samples must be multiplied in order to correct, on the average, for systematic errors.

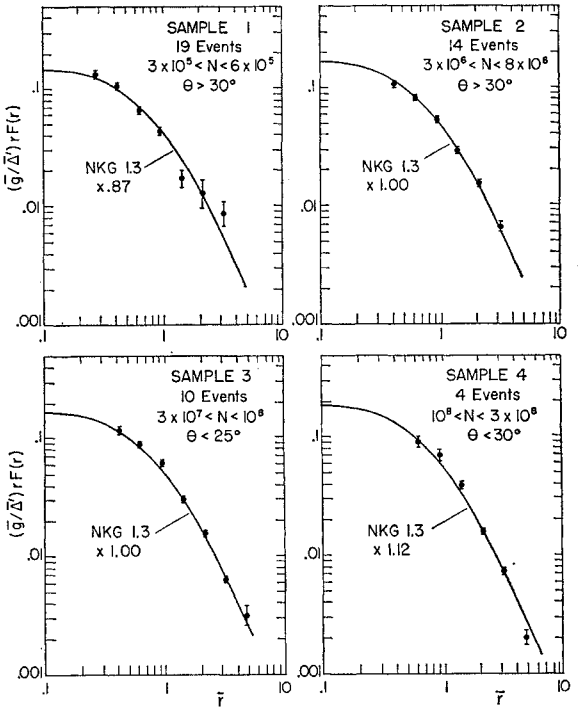

FIG. 9. Average lateral distributions for four samples of showers with widely different ranges of size and zenith angle. The curves all represent the function NKG 1.3 multiplied by factors so as to fit the data.

TABLE II. Specifications of the samples of real showers used in the determinations of the lateral distribution function.

Sample	Number of events	Nominal size interval	Zenith angle interval	Distance from center to core location	Trial function used in analysis
1	19	$3\times10^5<N<6\times10^5$	$\theta>30°$	<70 m	EXP
2	14	$3\times10^6<N<8\times10^6$	$\theta>30°$	<100 m	NKA 1.4
3	10	$3\times10^7<N<10^8$	$\theta<25°$	<190 m	NKA 1.4
4	4	$10^8<N<3\times10^8$	$\theta<30°$	<190 m	NKA 1.4

Information on the lateral distribution at distances small compared to the least separation between detectors is given only by showers that strike quite near some detector, so the number of available density measurements for small distances was not very great. Thus, for points very near the axis it was not possible to demonstrate that the measured lateral distribution was free from bias by the choice of trial function. Also, at such small distances random errors in core location became important. These considerations limit the range of our lateral distribution determinations to distances greater than 50 m. For the smallest showers, which were measured using the additional closely-spaced C detectors, the limit is about 20 m.

A potential source of systematic errors in the determination of the average structure function is the dependence of the calculated core location on the trial function. About 80 events were analyzed both with the EXP and with the NKA 1.4 trial functions. Within the M ring the displacements between the corresponding

calculated core positions are negligible. Near the D ring there is an obvious systematic displacement indicating that the EXP trial function tends to draw the core locations inward. The reason for this is that the EXP function falls considerably below the true structure function for $r>3.0$, so that the minimization routine tends to reduce the contributions to the deviation function from detectors at large distances by moving the calculated core location towards the center. On the other hand, the trial function NKA 1.4 is a better approximation to the true structure function than EXP, although its values at large distances are somewhat too large. In the analysis of the average structure function we minimized errors due to the uncertainties in core location by selecting showers as close to the center as possible. The small showers which were analyzed with the EXP trial function were used only if their cores struck within the M ring.

We tested the sensitivity of the above procedure to the choice of trial function by applying it to a sample of the showers which were analyzed with both the EXP and the NKA 1.4 trial functions. The sample consisted of those which fell within the M ring. The ratios of the calculated quantities $(\bar{g}/\bar{\Delta}')_n r_n F(r_n)$ for corresponding radial intervals obtained from the two analyses turned out to be nearly constant. Furthermore, neither set of quantities fitted the corresponding trial function well, whereas with appropriate fitting factors, they both fitted the function NKG 1.3. From these facts we conclude that the shape of the experimentally determined structure function is not seriously affected by the choice of trial function.

The errors in Fig. 9 include random instrumental errors and fluctuations in the numbers of particles that traversed the detectors, on the assumption that they have a Poisson distribution, calculated by the formula

$$\text{relative error}=\pm\left[\frac{1}{(\sum Ag)_n}+\frac{(0.15)^2}{P_n}\right]^{\frac{1}{2}}, \qquad (7)$$

where A is the area of a detector, $(\sum Ag)_n$ is the total number of detector traversals for the nth distance interval, P_n is the total number of density measurements in the interval, and 0.15 is the estimated instrumental error of a single density measurement.

We conclude that the function NKG 1.3 fits the average lateral distribution for showers ranging from size 5×10^5, inclination $>30°$, to size 10^8, inclination $<25°$. The agreement applies to distances $20<r<250$ m for the smaller showers, and for the larger showers, to distances $50<R<400$ m.

B. Fluctuations from the Average Lateral Distribution

In all of the preceding analysis it has been assumed that the fluctuations in the number of particles that traverse a detector have a Poisson distribution. This may not be so. It is conceivable that fluctuations in the development of a shower could give rise to local off-axis concentrations of particles which might, in extreme cases, constitute secondary cores. However, the apparent success of our data reduction method, in which number fluctuations are assumed to be Poisson, is indirect evidence for the correctness of that assumption. The fact that the data points of Fig. 9 lie on smooth curves within the errors shown indicates that the number fluctuations are not much worse than Poisson, since Poisson fluctuations were assumed in evaluating the errors. Other indirect evidence is given by the experimental ψ^2 distribution shown in Fig. 5. The average value of ψ^2 is 1.3, only slightly greater than the theoretical value of unity, which implies that the actual dispersion of the density measurements corresponds to the assumptions made in assigning the weights W_i. Direct evidence is given by Fig. 10 in which the individual calculated densities are based on NKG 1.3. The dashed lines on either side of the 45° line bound the region of one-standard-deviation fluctuations, where the standard deviation is based on Poisson density fluctuations plus 15% instrumental error. The fraction of points falling within the dashed lines is consistent with the assumption that the density fluctuations in air showers follow the Poisson distribution.

About one shower event in every 100 gave a very bad density fit ($\psi^2>4$). Investigation showed that some were very large showers ($N>10^8$) whose cores struck far outside the D ring. In such a case the machine computation would fail to converge in a reasonable number of steps. In other cases there was an anomalously large pulse from one detector. When the analysis was repeated omitting the anomalous datum the new fit was markedly improved. The most plausible explana-

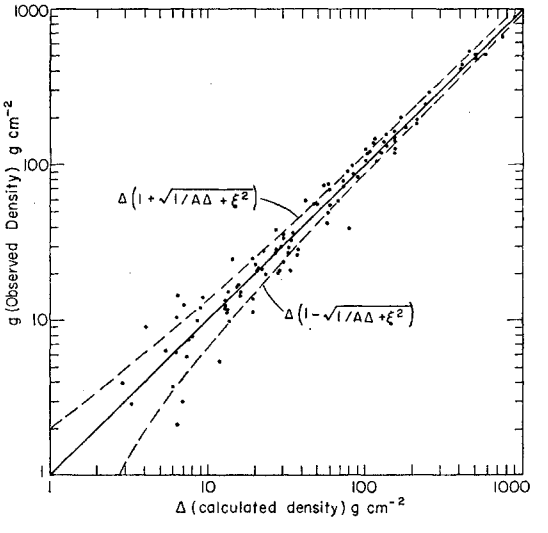

FIG. 10. Comparison between observed and calculated densities for 10 showers from sample 3. The dashed lines indicate one standard deviation of the Poisson distribution plus a 15% instrumental error.

TABLE III. Observed and calculated data on the largest shower observed. The large array is a tabulation of the observed arrival times and densities of the shower at each of the eleven detectors together with the corresponding expected values calculated from the parameter s, the size, and the core location which gave the minimum value of ψ^2 (indicated by an asterisk in the lower right-hand tabulation). Serial number 58042; date=March 1, 1957; time=20:24 EST.

Detector number	$c\times$observed arrival time (m)	$c\times$calculated arrival time (m)	Observed density (m^{-2})	Calculated density* (m^{-2})	Distance from axis (m)
1	852	856	128	163	367
2	839	872	5450	5600	129
3	839	837	2320	2420	169
4	801	800	160	150	376
5	791	809	76	68	464
6	887	843	445	470	274
7	867	850	3080	2710	163
8	844	837	2350	2270	172
9	803	821	396	436	280
10	823	826	250	241	330
11	844	852	672	780	237

Timing analysis	Density analysis				
	s	ψ^2	N ($\times10^9$)	Y (m)	Z (m)
Zenith angle=11°	0.9	1.28	8.08	−196	−157
Azimuth=15°	1.0	0.82	5.57	−195	−157
Rt. ascen.=112°	*1.1	0.55	3.49	−186	−151
Decl.=53°	1.2	0.70	2.36	−179	−146
χ=19 m	1.3	1.38	1.83	−176	−146
	1.4	2.51	1.50	−174	−146

tion of such events appears to be the occurrence of a nuclear interaction in the detector that gave the anomalous pulse. No significant indication of widely separated secondary cores was found.

C. Largest Shower

The largest shower recorded during the experiment was the one whose observed and calculated data are given in Table III. The core struck outside the D ring of detectors, so the core location cannot be as well determined as for the showers we normally accepted. Uncertainty in the core position is reflected in corresponding uncertainty regarding the shower size. Also, there is a question whether the lateral distribution of such a large shower is the same as for the smaller showers discussed previously, and the value obtained for the shower size depends rather sensitively on the choice of lateral distribution function.

The degree of uncertainty in the size can be estimated using $\psi^2=2$ as a confidence limit. Referring to Fig. 5, about 90% of the events have $\psi^2<2$. Analyses of the shower in question using the NKGs function for various s values gave the results summarized in Table III. The best fit was obtained for $s=1.1$, and the corresponding value of N is 3.5×10^9. However, a satisfactory fit was also obtained for $s=1.3$, in which case the value of N is 1.8×10^9.

In view of this large uncertainty in N it is appropriate to take into account the greater *a priori* probability of detecting smaller showers. To do this requires extrapolating the size spectrum to the region of interest in this case. The maximum likelihood size value, considering s values from 1.3 to 1.1 equally probable but smaller N values more probable than large, is 2×10^9, corresponding to $s=1.25$.

Figure 11 is a contour map of the ψ^2 hypersurface calculated for NKG 1.1. Also shown are the successions of core location approximations made by the computer during two minimizations of ψ^2 carried out by slightly different procedures. It is evident that for $s=1.1$ the core location could be displaced about 40 m towards the center of the array without causing the value of ψ^2 to exceed 2. The size value corresponding to such a core location would again be about 2×10^9. For larger s values the $\psi^2<2$ criterion permits less freedom in locating the core, so the combined effect of changing the core location and varying the value of s is not significantly different from that of changing s alone. Consequently, we adopt as our best value for the nominal size of shower number 58042 the figure 2×10^9 particles. The corresponding value for the "Geiger tube size" is 2.6×10^9 particles. The true value could be considerably larger but is unlikely to be appreciably smaller.

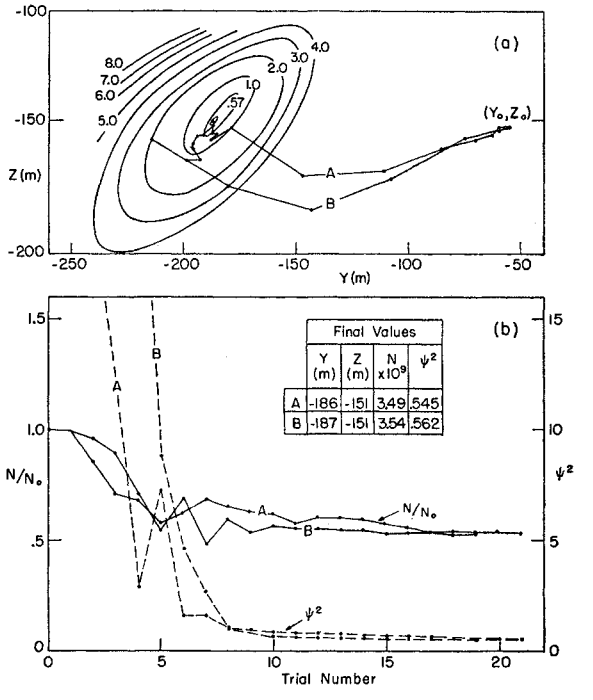

FIG. 11. (a) Contour map of the ψ^2 hypersurface calculated for shower number 58042 using trial function NKG 1.1. Successive core locations are shown for two stepwise minimizations of ψ^2. For the two analyses, A and B, the same trial function NKG 1.1 and the same initial estimates were used, but sizes of the initial steps were different. (b) Successive values of N and ψ^2 for analyses A and B. Final values are given in the inset table.

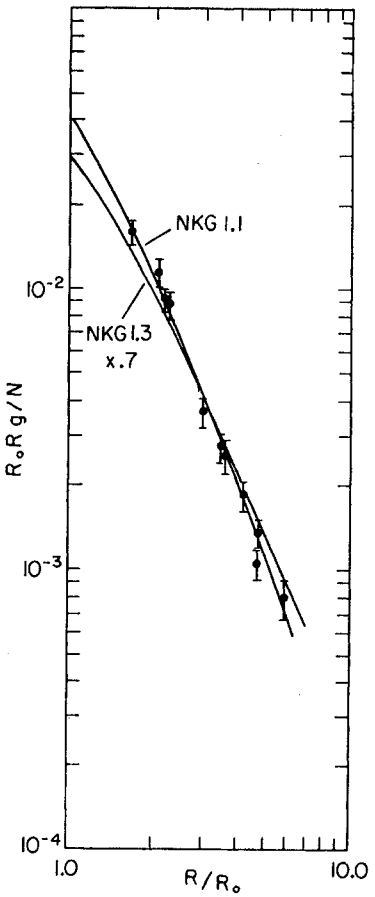

FIG. 12. Lateral distribution of the largest shower observed in this experiment. The smooth curves represent NKG 1.1 and NKG 1.3.

Figure 12 shows the experimental lateral distribution for this shower together with graphs of NKG 1.1 and NKG 1.3.

D. Distributions in Size and Zenith Angle

We define the differential shower size spectrum to be $s(N,x_0,\theta)$ such that $s(N,x_0,\theta)AdNd\Omega$ is the number per unit time of showers with size values in the range dN whose axes intersect the perpendicular area A at atmospheric depth x_0 (in g cm^{-2}) and are inclined at zenith angle θ within the solid angle element $d\Omega$. Assuming that the development of a shower depends on the total thickness of air traversed but not on the distribution of air density along its path, we can write $s(N,x_0,\theta)=s(N,x)$, where $x=x_0/\cos\theta$ is the thickness of the atmosphere along the direction of the shower axis. This assumption is well justified although not rigorously correct because of the occurrence of unstable particles in showers.

The recorded showers constitute biased samples from the distribution $s(N,x)$. Our problem is to evaluate the experimental bias so that the properties of $s(N,x)$ can be determined from the characteristics of the sample.

1. Selection Criteria and Acceptance Areas

The shower events we used in determining the size and zenith angle distributions constituted three groups corresponding to three size ranges. Showers recorded while the C detectors were in operation formed the first group. The second consisted of all showers selected electronically during a small portion of the period of operation with no C detectors. The third consisted of all the larger showers recorded during the balance of the period of operation. As we mentioned earlier, the electronic selection criterion, which we call C_1, required that three or more detectors register densities greater than a set value. Showers of the third group were selected by imposing a similar but stricter criterion C_2 while scanning the photographic records. Inclined showers of actual size N were more likely to be accepted by C_1 and C_2 than vertical showers because of the reduction in the separation between detectors when the array is projected onto the shower plane. We made the final selection for each group by accepting only those showers whose calculated sizes and core locations were such that their *a priori* probabilities for passing C_1 and C_2 were nearly unity. Thus the over-all experimental bias was determined essentially by the final selection criterion which we call C_3. Table IV summarizes the criteria and Fig. 13 summarizes the observed data. In these figures each event is represented by a point whose ordinate is the observed nominal size and

TABLE IV. Summary of criteria for selecting samples of showers used in determining the distributions in size and zenith angle.

	Criterion	Sample 1	Sample 2	Sample 3
C_1	Detectors included in the electronic triggering requirement	3 in rings *CE, C, M*	3 in rings *CE, M, D*	3 in rings *CE, M, D*
	Number of particles corresponding to the minimum pulse height required from detectors included in triggering	10	10	10
C_2	Detectors included in the preliminary selection requirement	···	···	3 in rings *M, D*
	Number or particles corresponding to minimum pulse height required from detectors included in selection	···	···	25
C_3	Detectors required to be within acceptance radius from calculated core position	3 in rings *CE, C, M*	3 in rings *CE, M, D*	3 in rings *M, D*
	Lateral distribution function used to calculate acceptance radius R_0	EXP	NKA 1.4	NKA 1.4
	Required calculated number of particles at perpendicular distance from axis equal to R_0	18	20	35
	Total yield	154	152	169

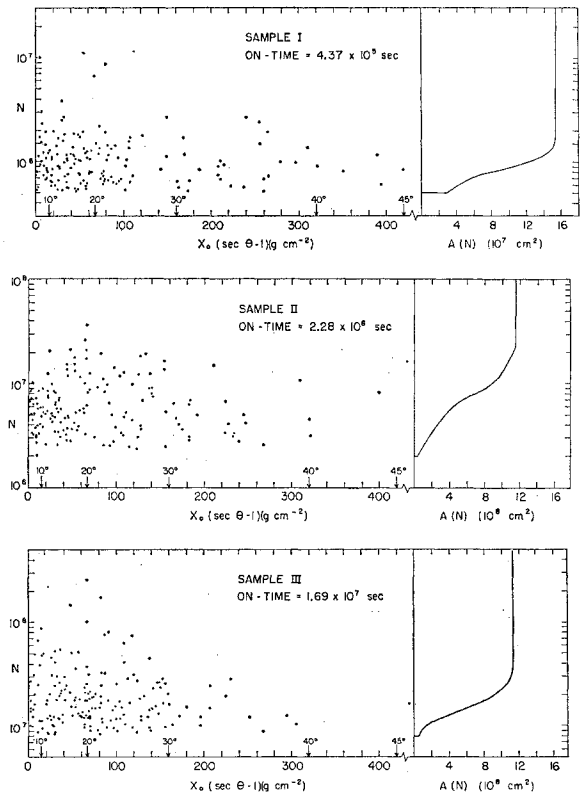

FIG. 13. Individual values of size and zenith angle for showers used in determination of the size spectrum. The three samples were selected according to the criteria listed in Table IV. The acceptance area $A(N)$ for each sample is plotted on the right-hand side.

whose abscissa is the atmospheric depth $x=x_0 \sec\theta$, where θ is the zenith angle.

The final selection criterion C_3 was, specifically, that the calculated core location of a recorded shower of given calculated size had to lie in such a position that the expected density at three or more detectors for a vertical shower of the same size and core location would be at least 2.0 standard deviations more than the minimum densities required by C_1 and C_2. In addition, the calculated core location had to lie within a certain fixed distance of the center detector so that only showers with well determined core locations and sizes were accepted. To each size N there corresponded a certain area $A(N)$, called the acceptance area within which any shower of calculated size N was accepted, and within which the *a priori* probability for a shower of actual size N to pass C_1 and C_2 was nearly unity. With this procedure, the effective horizontal area for the detection of showers of actual size N and any inclination was very nearly $A(N)$.

In practice, $A(N)$ was calculated as a function of N in two steps. We first calculated an acceptance radius $r(N)$ which we call the perpendicular distance from the axis of a shower of size N at which the particle density according to the trial function equals the minimum density required by C_3. For a given size N we drew circles with radii equal to $r(N)$ centered on each of the detectors included in the specification of C_3, and directly measured $A(N)$ which is equal to the area enclosed within any three circles and within the specified outer boundary. We determined the acceptability according to C_3 of a given shower of size N by drawing a circle of radius $r(N)$ around the calculated core location. If the required number of detectors was included within the circle, the shower was accepted.

We can now construct an expression which relates the expected experimental results to the basic distribution function s in terms of the acceptance area A. We call $\Phi(N,x)dNdx$ the expected number of accepted showers that have sizes between N and $N+dN$ and zenith angles corresponding to atmospheric thicknesses between x and $x+dx$. We then have the relation

$$\Phi(N,x)dNdx = TA(N)s(N,x)(2\pi x_0^2/x^3)dxdN, \qquad (8)$$

where T is the time of observation. We note that the quantity $(x_0/x)A(N)$ is the projected acceptance area on a plane perpendicular to the shower axis, and the quantity $(2\pi x_0/x^2)dx$ is the solid angle contained within the corresponding differential interval of zenith angle.

2. *Zenith Angle Distribution. Dependence of $s(N,x)$ on x*

The general form of the dependence of $s(N,x)$ on x can be seen in the plots shown in Fig. 14. These plots were prepared for each of the three groups of showers as follows. We designated four equal intervals of x over the range from $x=x_0$ to $x=1.287x_0$ (corresponding to the range of zenith angles $0\leqslant\theta<39°$) and assigned each event with x in this range to one of four subgroups, depending on which interval the calculated value of x fell into. For each subgroup we then found the sum of the values of $(x/x_0)^3$, and plotted the logarithm of this sum as ordinate *vs* the value of the interval as abscissa. The expectation value of this sum at the midpoint for a given depth interval Δx is proportional to the average intensity in the interval averaged over a range of sizes determined by the function $A(N)$. To see this we multiply both sides of Eq. (8) by $(x/x_0)^3$ and integrate with respect to N and x to obtain the relation

$$\int_x^{x+\Delta x}(x'/x_0)^3\left[\int_0^\infty \Phi(N,x')dN\right]dx' = (2\pi T/x_0)\int_x^{x+\Delta x}\left[\int_0^\infty A(N)s(N,x')dN\right]dx'. \qquad (9)$$

The left-hand term of Eq. (9) is the expectation value of the experimentally determined sum. The expression $A(N)s(N,x')dN$ may be thought of as the intensity of showers at depth x' as seen through a "filter" represented by the response function $A(N)$ which determines the distribution in size of the recorded showers. In the

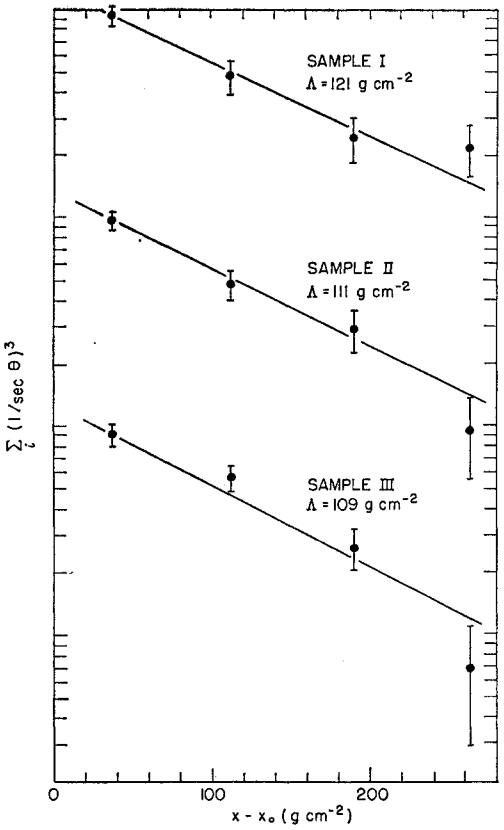

FIG. 14. Variation of shower intensity with atmospheric depth. The straight lines represent exponential variation. Their slopes were calculated by the method of maximum likelihood.

limit as the number of data increases and as $\Delta x \rightarrow 0$, this procedure would yield an experimental quantity that is proportional to the intensity of showers at the depth x averaged over the sizes transmitted by the filter. In practice, it is necessary to take large intervals of x in order to obtain statistically significant results, and we chose intervals of x equal to 75 g cm^{-2}. The three plots in Fig. 14 show a similar exponential form in spite of the fact that the showers in the three groups have very different average sizes, namely about 6×10^5, 5×10^6, and 5×10^7. This observation is consistent with the assumption that dependence of $s(N,x)$ on x can be represented approximately by the exponential relation

$$s(N,x)\sim\exp[-(x-x_0)/\Lambda], \qquad (10)$$

with Λ constant from $N=5\times10^5$ to about 5×10^7. To verify this, we substitute this expression for $s(N,x)$ in the right-hand side of Eq. (9) which then becomes proportional to $\exp[-(\bar{x}-x_0)/\Lambda]\sinh(\Delta x/2\Lambda)$, where $\bar{x}=x+\Delta x/2$. Since Δx is the same for the four intervals of x, it follows that the expectation values of the sums of $(x/x_0)^3$ depend exponentially on the mean values of x for the intervals. The slopes of these semi-logarithmic plots are therefore direct measures of the characteristic attenuation length Λ of the shower intensity.

The maximum likelihood value of Λ for each group was calculated on the assumption that the dependence of s on x can, indeed, be expressed by Eq. (10), and that Λ is a constant for each group. The values we obtain are indicated by the slopes of the lines drawn on the plots in Fig. 14. From the combined data we conclude that the zenith angle distribution of showers with nominal sizes in the range from 5×10^5 to 5×10^7 can be represented by Eq. (16) with $\Lambda=113\pm9$ g cm^{-2}. The error indicates both the systematic uncertainties and the statistical error.

3. *Size Distribution. Dependence of $s(N,x)$ on N*

We have established that the dependence of $s(N,x)$ on x can be separated from its dependence on N within the accuracy of our data over the range of nominal sizes from 5×10^5 to about 5×10^7. For the determination of the size distribution up to 5×10^7 particles, we shall therefore lump together all events without regard to their zenith angles.

The expected number of showers with nominal sizes between N and $N+dN$ that would be recorded with our apparatus during a given time T can be expressed by the relation

$$\int_{x_0}^{\infty}\Phi(N,x)dNdx=TA(N)\Omega_{\text{eff}}s(N,x_0)dN, \qquad (11)$$

where Ω_{eff}, which we call the effective solid angle, is defined by the equation

$$\Omega_{\text{eff}}=2\pi\int_{x_0}^{\infty}(x_0^2/x^3)\exp[-(x-x_0)/\Lambda]dx. \qquad (12)$$

To find $s(N,x)$ we proceed as follows. To each event we assign a statistical weight equal to the quantity $[T\Omega_{\text{eff}}A(N)]^{-1}$, and we find the sum of the statistical weights of the events in each of several size intervals. The expectation value of this sum divided by the size interval is equal to the average value of the size distribution in this interval as can be seen by rearranging Eq. (11) and integrating over N to obtain the relation

$$(\Delta N)^{-1}\int_N^{N+\Delta N}\left\{[T\Omega_{\text{eff}}A(N')]^{-1}\int_{x_0}^{\infty}\Phi(N',x)dx\right\}dN' = (\Delta N)^{-1}\int_N^{N+\Delta N}s(N',x_0)dN'. \qquad (13)$$

In the limit as the number of data increases and as $\Delta N\rightarrow0$, this procedure would, in principle, yield an experimental value of the differential spectrum for the size N. In practice, it is necessary to take large intervals of N in order to obtain statistically significant results. We have, correspondingly, chosen intervals of N which

TABLE V. Summary of the experimental results on the absolute intensity of showers with nominal sizes between 5×10^5 and 5×10^8 particles.

Interval No.	Nominal size range ($\times10^6$)	$(\Sigma_j A_j^{-1})/\Omega_{\text{eff}}T\Delta N$ (cm^{-2} sec^{-1} sterad^{-1}) Sample 1 $T=4.37\times10^5$ sec	Sample 2 $T=2.28\times10^6$ sec	Sample 3 $T=1.69\times10^7$ sec	$\Sigma_j \mathfrak{A}_j^{-1}/(T\Delta N)$ (cm^{-2} sec^{-1} sterad^{-1}) Sample 3 (VES) $T=1.69\times10^7$ sec	$\bar{N}$ ($\times10^6$)	S (cm^{-2} sec^{-1} sterad^{-1})
1	0.5–1	1.26×10^{-17} (83)				0.7	$(1.3\pm0.3)\times10^{-17}$
2	1–2	1.90×10^{-18} (62)				1.4	$(1.9\pm0.4)\times10^{-18}$
3	2–4	1.28×10^{-19} (9)	1.14×10^{-19} (45)			2.8	$(1.2\pm0.3)\times10^{-19}$
4	4–8		3.25×10^{-20} (60)			5.6	$(3.3\pm0.7)\times10^{-20}$
5	8–16		4.32×10^{-21} (36)	5.45×10^{-21} (81)		11.2	$(5.1\pm0.9)\times10^{-21}$
6	16–32		5.16×10^{-22} (11)	4.68×10^{-22} (62)		22.4	$(4.7\pm0.9)\times10^{-22}$
7	32–64			5.25×10^{-23} (17)		45	$(5.3\pm1.5)\times10^{-23}$
8	64–128			9.25×10^{-24} (6)	9.30×10^{-24} (9)	90	$(9.3\pm3.4)\times10^{-24}$
9	128–256			2.35×10^{-24} (3)	2.07×10^{-24} (4)	180	$(2.1\pm1.0)\times10^{-24}$
10	256–512				5.15×10^{-25} (2)	360	$(5.2\pm3.9)\times10^{-25}$

cover factors of 2; i.e., for each interval $\Delta N=N$. We list the experimental results in Table V in the columns labeled samples 1, 2, and 3. These results are derived from the data on accepted showers which are summarized in Fig. 13. The quantities in parentheses indicate the numbers of accepted showers on which each quoted value is based.

The next step in the analysis of the size distribution is to plot the logarithm of the tabulated intensities vs the number labeling the corresponding size interval. The points in this plot fall close to a straight line with a slope of 2.90. Since the size intervals are equal logarithmic intervals, this result is consistent with the assumption that the dependence of $s(N,x)$ on N can be represented approximately by the power law relation

$$s(N,x_0)\propto N^{-(\Gamma+1)}, \tag{14}$$

with $\Gamma=1.90$.

Showers with more than 5×10^7 particles were not recorded in sufficient numbers to permit us to determine whether or not their zenith angle and size dependences can be separated from one another, as could those of showers with sizes from 5×10^5 to 5×10^7. A change in Λ with shower size, and therefore a change in the effective solid angle Ω_{eff} could be caused by a change in either the absorption characteristics of showers or by a change in the primary energy spectrum. Since we wished particularly to explore the primary spectrum for very high energies, it was desirable to avoid an analysis based on the untested assumption that Λ remained constant. One way to have avoided this difficulty would have been to confine our attention to events with arrival directions so near the vertical that a knowledge of the form of the zenith angle dependence would not have been important in determining the effective solid angle. Unfortunately, the scarcity of very large events precluded such an approach. Instead, we extended the size spectrum beyond 5×10^7 by a method based only on the plausible assumption that the atmospheric attenuation of showers does not change drastically in the size range from 5×10^7 to 5×10^8.

For this analysis we define the "vertical equivalent size" by the equation

$$N_v=N\exp[(x-x_0)/\lambda]. \tag{15}$$

It follows from Eqs. (10), (14) and (15) that in their region of validity

$$s(N,x_0)dN_v=s(N,x)dN. \tag{16}$$

We note that there exists between s, N, and x the identity relation

$$(1/N)(\partial N/\partial x)_s = -[(1/s)(\partial s/\partial x)_N/(N/s)(\partial s/\partial N)_x]. \tag{17}$$

According to the experimental results expressed by Eqs. (10) and (14), the right-hand term of Eq. (17) has a constant value of $-(1/\Gamma\Lambda)$ over the range of N up to 5×10^7. In the absence of fluctuations the left-hand term would be the reciprocal logarithmic slope of the curve representing the number of particles in a given shower as a function of depth, and it would, therefore, be independent of the primary spectrum. This conclusion is still valid to a fair approximation, even in the presence of fluctuations. We therefore use for λ in Eq. (15) the value of $\Gamma\Lambda$ determined for $N<5\times10^7$, namely $\Gamma\Lambda=214$ g cm^{-2}.

We now assume that the above value of λ is valid for $N>5\times10^7$. For each shower we calculate the value of N_v according to Eq. (15). In order to reduce uncertainties due to errors in x and Λ, we consider only showers with zenith angles less than 30°. From Eqs. (8) and (15) we find that the expected number of showers with N_v in the interval dN_v is

$$\int_{x_0}^{x_0\sec\theta}\Phi(N_v\exp[-(x-x_0)/\Gamma\Lambda],x)dxdN_v = T\mathfrak{A}(N_v)s(N_v,x_0)dN_v, \tag{18}$$

where we define $\mathfrak{A}(N_v)$ by the equation

$$\mathfrak{A}(N_v)=\int_{x_0}^{x_0\sec\theta}A(N_v\exp[-(x-x_0)/\Gamma\Lambda])\times2\pi(x_0^2/x^3)dx. \tag{19}$$

It turns out that $\mathcal{A}(N_v)$ is constant for the observed showers with $N>6.4\times10^7$ particles. We assign to each event with $N_v>6.4\times10^7$ a statistical weight equal to $[T\mathcal{A}(N_v)]^{-1}$, and find the sum of the statistical weights of the events in each size interval divided by the size interval. The expectation value of this quantity is

$$(\Delta N)^{-1}\int_N^{N+\Delta N}\left\{[T\mathcal{A}(N_v)]^{-1}\times\int_{x_0}^{x_0\sec\theta}\Phi(N_v\exp[-(x-x_0)/\Gamma\Lambda],x)dx\right\}dN_v$$
$$=(\Delta N)^{-1}\int_N^{N+\Delta N}s(N_v,x_0)dN_v, \quad (20)$$

and it approaches $s(N,x_0)$ as the size interval is narrowed. Consequently, the calculated sums are entirely analogous to those previously listed, and they are listed in Table V in the column labeled sample 3 (VES).

Before the data in Table V can be plotted as a size spectrum, it is necessary to find for each interval the value of N for which the intensity would be equal to the average intensity for the interval. This value, which we call $\bar{N}$, is given by the equation

$$\bar{N}^{-(\Gamma+1)}=(\Delta N)^{-1}\int_{N_1}^{N_1+\Delta N}N^{-(\Gamma+1)}dN. \quad (21)$$

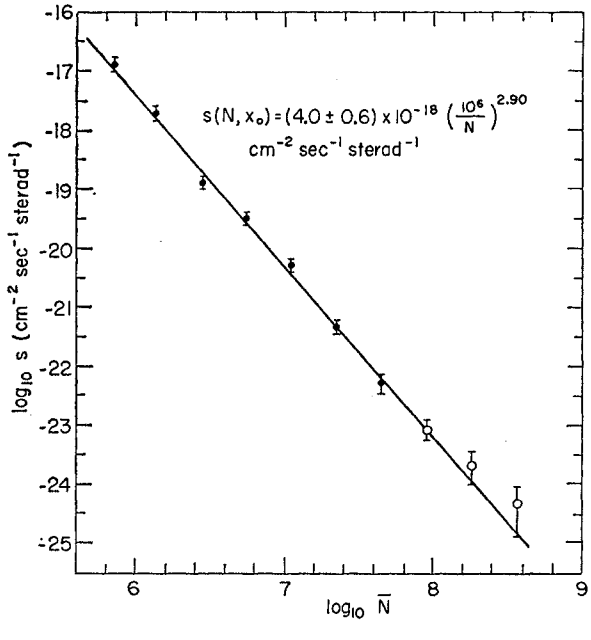

FIG. 15. Variation of the absolute differential shower intensity with nominal size. The intensity for a given Geiger tube size is larger than for the same nominal size by the factor 1.65.

For our case, with $\Delta N=N_1$, and $\Gamma=1.90$, we have $\bar{N}=1.39N_1$.

Figure 15 is a plot of s vs $\bar{N}$. The indicated fractional errors have been set equal to $(1/n+0.15^2)^{\frac{1}{2}}$, where n is the number of events on which the value of s is based, and 0.15 is a rough estimate of the error due to experimental uncertainties.[10] The straight line in Fig. 15 indicates the power law that best fits the data.

Up to this point the size values dealt with in calculating intensities have been the nominal sizes given by our routine calibration procedure. In order to simplify comparisons between this and other work it is useful to express intensities in terms of shower sizes as they would be measured by standard Geiger tube techniques. Our measurement described in Sec. II-B indicates that the "Geiger tube size" of a shower, which we will denote by N', is larger than our nominal size by a factor of 1.3. Therefore the intensity for a given Geiger tube size spectrum can be represented by the same power law multiplied by the factor $(1.3)^{1.9}=1.65$.

In summary, we find that the dependence of the differential shower intensity on Geiger tube size and atmospheric depth is described by the following formula, which is valid for N' in the range 7×10^5 to 7×10^8 and x in the range 1040 g cm^{-2} to 1340 g cm^{-2}:

$$s(N',x)=s_0(10^6/N')^{\Gamma+1}\exp[-(x-x_0)/\Lambda], \quad (22)$$

where $s_0=(6.6\pm1.0)\times10^{-8}$ cm^{-2} sec^{-1} sterad^{-1}, $\Lambda=(113\pm9)$ g cm^{-2}, and $\Gamma=1.90\pm0.10$. If we call $S(N',x_0)$ the vertical intensity of showers with Geiger tube sizes greater than N' at sea level, we find from Eq. (22) that

$$S(N',x_0)=S_0(10^6/N')^{\Gamma}, \quad (23)$$

where $S_0=(3.5\pm0.5)\times10^{-12}$ cm^{-2} sec^{-1} sterad^{-1} (or, approximately, $S_0=1$ m^{-2} year^{-1} sterad^{-1}).

As mentioned earlier, the largest shower that we recorded during the total period of operation (1.69×10^7 sec) had an estimated nominal size of 2×10^9 particles. The core location lay outside the largest acceptance area so that it was not included in the data from which the above size spectrum was derived. However, we made an estimate of the expected number of events with $N'>10^9$ that would have passed criteria C_1 and C_2 of sample 3 during the entire time of operation on the assumption that the spectrum is valid for all sizes. Any such event would have been conspicuous either by virtue of its large calculated size or, in case the core location lay far outside the array, by failure of the computation routine to reach an acceptably small value of ψ^2. The area within which events with $N'>10^9$ would certainly have been detected was about 10^{10} cm^2.

[10] A part of this uncertainty is due to the finite size resolution, which may lead to systematic errors in the determination of intensities in those ranges of size where the frequency of accepted showers varies rapidly. In our case, the frequency of accepted showers increased with size in some intervals and decreased in others so that the evaluation of this error is difficult. A reasonable upper limit for this error appears to be ±15%. Because of its smallness we have merely included it in the over-all estimate of error.

According to our extrapolation of Eq. (23), the expected number of such events would be about 0.7. The fact that we observed one such event and that its size was actually twice 10^9 is evidence against any sizable steepening of the size spectrum in the region $5\times10^8<N'<2\times10^9$.

E. Celestial Arrival Directions

Figure 16(a) shows the distribution of arrival directions for the showers accepted by C_1 and C_2 of sample 3 (but not necessarily by C_3). The average size of these showers is 1.8×10^7. The time of observation was the same to within 10% for any set of equal sidereal time intervals. Thus, in the absence of any anisotropy the expected density of points along any line of constant declination should be a constant. We therefore performed a chi-square test on the observed numbers of events in each $10°\times10°$ region along a declination band and found that the results were consistent with the hypothesis of isotropy. We also compared the observed numbers of events from special regions in the sky with the numbers that would be expected if the distribution were isotropic. The regions tested were: (1) a 20° band centered on the galactic plane; (2) a 20° band centered on the plane perpendicular to the local spiral arm of the galaxy; (3) a 40° $\times$40° region centered on the direction along the spiral arm near $\alpha=300°$, $\delta=+35°$. The expected and observed numbers of events are listed in Table VI. No significant anisotropy is evident.

In order to study the arrival directions of the most energetic showers, we computed the vertical equivalent size of all large showers in the same group as above. Figure 16(b) is a plot of the arrival directions of the showers with $N_v>10^8$. Again, we consider that no significant anisotropy is evident.

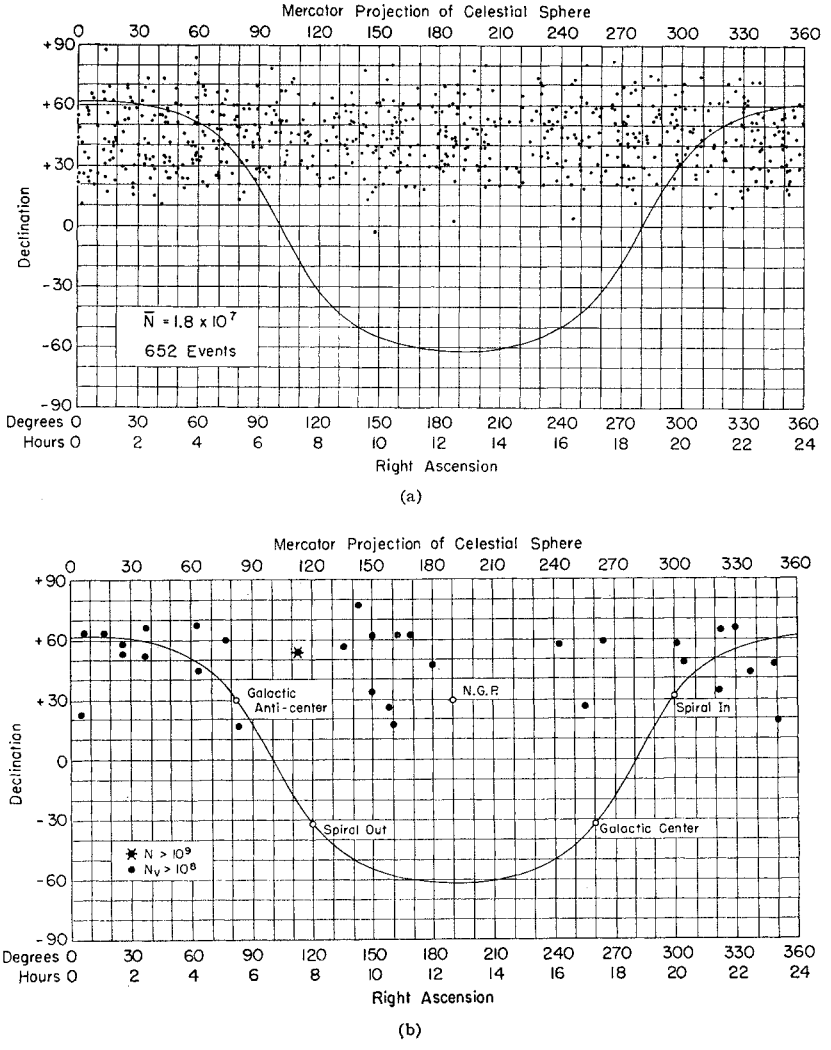

FIG. 16. Distributions of arrival directions for the largest showers. The average size of the showers plotted in (a) was 1.8×10^7. Only showers with $N_v>10^8$ are plotted in (b). The largest shower (number 58042) is indicated by the star.

TABLE VI. Summary of the observed numbers of events with an average size of 1.8×10^7 from several special regions of the sky together with the numbers expected according to the hypothesis that the directions of the primaries are isotropically distributed.

Region examined	Number of events Expected	Observed
Galactic plane	128	135
Plane perpendicular to spiral arm	117	126
Direction along spiral arm, $\alpha=300°$, $\delta=35°$	57	49

IV. INTERPRETATION OF THE RESULTS

A. Energy Spectrum of the Primary Particles

We shall determine an approximate expression for the high-energy spectrum of the primary particles from our results on the size spectrum. We call $J(E)$ the intensity of primary particles with energy greater than E. If fluctuations in the development of showers were negligible, then every primary of energy E would give rise to a shower of unique size $N(E,x)$ at depth x in the atmosphere. The relation between J and S would then be simply

$$J(E)=S[N(E,x),x]. \tag{24}$$

However, fluctuations are not negligible and the most important ones are probably those that occur in the early stages of development, particularly fluctuations in the atmospheric depth of the first interactions of the primary particles. We therefore carry out an approximate evaluation of the primary spectrum taking into account only the latter source of fluctuations and using theoretical results on the average development of showers.

Since we neglect all fluctuations except those in the depth of the first interaction, we may define a quantity $n(E,u)$ to be the exact number of particles in a shower initiated by a primary particle of energy E whose first interaction occurs at a height u (measured in g cm^{-2}) above the point of observation. Calculations, which have been carried out for various models of high-energy nuclear interactions, yield the average number $N(E,x)$ of particles in a shower at the depth x below the top of the atmosphere generated by a primary particle of energy E. N and n are related by the equation

$$N(E,x)=[(1-\exp(-x/l)]^{-1}\times\int_0^x n(E,u)\exp[-(x-u)/l]du/l, \tag{25}$$

where l is the collision mean free path of the primary particles, and $[1-\exp(-x/l)]^{-1}\exp[-(x-u)/l]du/l$ is the probability that the first interaction takes place at the height between u and $u+du$ above the point of observation. Differentiation of Eq. (25) with respect to x gives the relation

$$n(E,x)=\left(1+l\frac{\partial}{\partial x}\right)N(E,x), \tag{26}$$

where the term $\exp(-x/l)$ has been ignored since it is negligibly small compared to unity at sea level.

The integral intensity of showers with sizes greater than n at depth x which are initiated by primaries that interact in a layer of thickness du at a height u above the point of observation is $J(E(n,u))\exp[-(x-u)/l]du/l$, where $E(n,u)$ in the inverse function of $n(E,u)$ and represents the energy of the primary of a shower that has exactly n particles at a depth u below the first interaction. Thus, the integral intensity of all showers with sizes greater than n is

$$S(n,x)=\int_0^x J(E(n,u))\exp[-(x-u)/l]du/l. \tag{27}$$

Differentiation of Eq. (27) with respect to x gives the relation

$$J(E)=\left(1+l\frac{\partial}{\partial x}\right)S(n(E,x),x). \tag{28}$$

Equation (28) together with Eq. (26) specifies the transformation by which the observed size spectrum S is related to the primary energy spectrum. The quantities S and $\partial S/\partial x$ are directly available from our experimental results, whereas l, N, and $\partial N/\partial x$ must be inferred from this and other experiments, and from theoretical considerations.

Most theoretical models of shower development share the general property that for showers with sizes less than 10^8 particles at sea level the logarithmic derivative of N with respect to x is slowly varying with x and E. It is convenient therefore to characterize the dependence of N on x by the quantity λ which we define by the equation

$$1/\lambda=-(1/N)(\partial N/\partial x), \tag{29}$$

where in general λ is a function of E and x. Our experimental results indicate that over the range of sizes from 10^6 to 10^8 particles the logarithmic derivative of S with respect to x is approximately constant. We therefore have the relation

$$1/\Lambda=-(1/S)(\partial S/\partial x). \tag{30}$$

Combining Eqs. (26), (28), (29), and (30), we obtain

$$J(E)=(1-l/\Lambda)S[(1-l/\lambda)N(E,x),x]. \tag{31}$$

Two features of the relation between J and S are of particular interest. One of these is that it is very sensitive to the value of l since l/Λ is not much less than one. Indeed, if it were found that $\Lambda=l$ for sizes greater than some value N_c, then one would conclude that $J(E_c)=0$ where E_c is the primary energy corre-

sponding to showers with an average size of N_e. The other feature is that its sensitivity to Λ and λ can be reduced by making observation where these quantities are large; i.e., at altitudes where the observed showers are near their maxima. In the limiting case where $\Lambda=\infty$ and $\lambda=\infty$, the relation between J and S would be Eq. (24).

We now apply Eq. (31) to the interpretation of our size spectrum using the theoretical results of Olbert[11] on the development of showers according to a model of high-energy nuclear interactions which he designates as Landau-model A with 50% elasticity and a collision mean free path of 70 g cm^{-2}. For this model he finds at sea level

$$N=1.7\times10^5(E/10^{15})^{1.14}, \tag{32}$$

where E is expressed in ev. The range of Geiger tube sizes well covered by our data is from 7×10^8 particles so that the corresponding energy range is 3×10^{15} to 10^{18} ev. At sea level the theoretical value of λ for this model varies from about 170 to 280 g cm^{-2} over this range of energy. In fact, this variation is so slow that it can be neglected without introducing errors larger than the experimental uncertainties. We shall therefore assume for λ a constant value $\Gamma\Lambda$ where Γ and Λ have the values found previously. Taking $l=70$ g cm^{-2}, $\Lambda=113$ g cm^{-2}, and $\lambda=214$ g cm^{-2}, we find

$$J(E)=J_0(10^{15}/E)^{\gamma}\ \text{cm}^{-2}\ \text{sec}^{-1}\ \text{sr}^{-1}, \tag{33}$$

with $J_0=(8.2\pm3.1)\times10^{-11}$ cm^{-2} sec^{-1} sterad^{-1}, and $\gamma=2.17\pm0.1$. This expression is valid in the energy range from 3×10^{17} ev to 10^{18} ev.

The fact that we detected a shower with a Geiger tube size of 2.6×10^9 indicates that the above spectrum may be valid for energies above 10^{18} ev. According to Eq. (32) the energy of the primary particle that produced this shower was 4.7×10^{18} ev. The corresponding figure for a purely electromagnetic cascade (photon-induced) would be 3.6×10^{18} ev, according to the calculation of Snyder.[12] Olbert's calculations place a lower limit of 2.8×10^{18} ev on the primary energy for any reasonable assumed model of high-energy nuclear interactions. One reason for the close agreement of widely different models is that all models agree in predicting that a vertical shower of this size is near maximum development at sea level.

At the present time the most plausible explanation of the production of ultra-high-energy cosmic rays is that they acquire their energy through a process of gradual acceleration in regions of hydromagnetic turbulence as first suggested by Fermi.[13] During their acceleration the particles diffuse over a space whose linear dimensions are large compared to the radii of curvature of the particles. According to this picture, the existence of particles of a given energy sets a corresponding lower limit on the dimensions of the space within which the particles acquire their energy. A plausible value for the average strength of the galactic magnetic field is 3×10^{-6} gauss.[14] If the shower referred to above was initiated by a proton, and if we use the figure 4.7×10^{18} ev as the most likely value of its energy, then its average radius of curvature in the galactic magnetic field was about 5000 light years (l.y.). The diameter of even the galactic halo is not very large compared to this figure so that an extra-galactic origin may be indicated for the most energetic cosmic rays. Of course, if the primary in this case was a heavy nucleus, then the radius of curvature would be reduced by a factor of Z, and this would reduce the strength of the evidence given by such events for the presence of cosmic-ray particles in space far from the narrow disk of the galaxy.

B. Isotropy of the Primary Flux

The absence of any significant anisotropy in the flux of high-energy primaries also places restrictions on possible models of cosmic-ray origin. If primaries of a given energy arrive isotropically, then the region of space around the earth which contains a uniform density of such particles must extend to distances which are large compared to the radius of curvature of the particles in the local magnetic field. Primaries that initiate showers with more than 10^8 particles have energies exceeding 2×10^{17} ev. If they are protons, and if the local galactic field has a strength of 3×10^{-6} gauss, their radius of curvature is 200 l.y. The observed isotropy of such particles indicates therefore that the region around the earth which contains a uniform intensity of such particles must extend considerably beyond 200 l.y. in all directions.

C. Important Role of the Nucleonic Cascade in the Development of Air Showers

Direct observations of nuclear interactions above 10^{13} ev in photographic emulsions, as well as detailed investigations of nuclear active particles in air showers, support the general view that high-energy nucleonic cascades penetrates great thicknesses of matter. We have presented our finding that a single function, NKG 1.3, describes the average lateral distribution for showers with widely different sizes and zenith angles. The NKG functions were derived theoretically to describe purely electromagnetic cascades, and the function NKG 1.3 specifically describes the lateral distribution for such cascade showers when they are "old," that is, when they are well past their maximum development.

[11] S. Olbert (private communication).
[12] H. S. Snyder, Phys. Rev. **76**, 1563 (1949).
[13] E. Fermi, Phys. Rev. **75**, 1169 (1949).
[14] V. L. Ginsburg, *Progress in Elementary Particle and Cosmic Ray Physics*, edited by J. G. Wilson and S. A. Wouthuysen (North-Holland Publishing Company, Amsterdam, 1956), Vol. IV, Chap. 5.

It has been pointed out frequently that the persistence of energetic nucleonic cascades provides an explanation for the fact that the lateral distribution of electrons in air showers is independent of size and zenith angle. The suggested interpretation is that an air shower at sea level is a composite of many old electromagnetic showers initiated by relatively low-energy γ rays. The γ rays arise from the decay of π^0 mesons which are produced along the axis of the shower in a high-energy nucleonic cascade that persists even to sea level. The shower of electrons is constantly replenished from the central core, and the total number of electrons at a given depth reflects the state of development of the dominant nucleonic cascade at somewhat smaller depths.

V. SUMMARY OF EXPERIMENTAL RESULTS

The following is a summary of our principal experimental results.

1. The existence of primary particles with energies greater than 10^{18} ev is established by the observation of one shower with more than 10^9 particles.

2. The function $f(r)=0.45(N/R_0^2)r^{-0.7}(1+r)^{3.2}$, where $r=R/R_0$ and $R_0=79$ m describes the average lateral distribution of shower particles at distances in the range $50\text{ m}<R<400$ m for showers with sizes in the range $5\times10^5<N<10^8$.

3. Over the same ranges in size and distance the density fluctuations in individual showers have a Poisson distribution.

4. The dependence of the absolute intensity of showers on N' and θ, the Geiger tube size and zenith angle, can be represented by the formula

$$s(N',x)=s_0(10^6/N')^{\Gamma+1}\exp[-(x-x_0)/\Lambda],$$

where $x=x_0\sec\theta$, $x_0=1040$ g cm^{-2}, $s_0=(6.6\pm1.0)\times10^8$ cm^{-2} sec^{-1} sterad^{-1}, $\Gamma=1.90\pm0.10$, $\Lambda=(113\pm9)$ g cm^{-2}, $x_0<x<1.3x_0$, and $7\times10^5<N'<7\times10^8$.

5. No evidence is found of anisotropy in the arrival directions or of a break in the energy spectrum of the primaries up to the largest energies observed.

6. Assuming a specific model for shower development and taking into account fluctuations in the depth of the first interaction, the integral energy spectrum of the primaries is

$$J(E)=J_0(10^{15}/E)^\gamma,$$

where $J_0=(8.1\pm3.1)\times10^{-11}$ cm^{-2} sec^{-1} sterad^{-1}, $\gamma=2.17\pm0.1$, and 3×10^{15} ev$<E<10^{18}$ ev.

ACKNOWLEDGMENTS

The important contributions of Professor P. Bassi and Professor M. Oda to the early stages of the planning and development of the experiment are gratefully acknowledged. The experimental site at the Agassiz Station of the Harvard College Observatory was made available through the courtesy of Harvard University. The authors express their thanks to the staff of the Observatory and to its director, Professor D. Menzel. Many members of the Laboratory for Nuclear Science of the Massachusetts Institute of Technology contributed their efforts to the experiment, and special thanks are due to Professor P. Demos and Dr. F. Eppling, and to W. Smith, C. Fernald, and V. Scrima. Members of the M.I.T. Computation Laboratory generously assisted us in our use of the Whirlwind and IBM-704 computers.